◆ Human Brain Mapping 35:3277–3289 (2014) ◆

Measurement and Genetics of Human Subcortical and Hippocampal Asymmetries in Large Datasets

Tulio Guadalupe,[1,2] Marcel P. Zwiers,[3] Alexander Teumer,[4] Katharina Wittfeld,[5] Alejandro Arias Vasquez,[6,7,8] Martine Hoogman,[1] Peter Hagoort,[3,9] Guillen Fernandez,[3,8] Jan Buitelaar,[7,8] Katrin Hegenscheid,[10] Henry Völzke,[11] Barbara Franke,[6,7,8] Simon E. Fisher,[1,12] Hans J. Grabe,[5,13] and Clyde Francks[1,12]*

[1]Language and Genetics Department, Max Planck Institute for Psycholinguistics, Nijmegen, The Netherlands
[2]International Max Planck Research School for Language Sciences, Max Planck Insitute for Psycholinguistics, Nijmegen, The Netherlands
[3]Centre for Cognitive Neuroimaging, Donders Institute for Brain, Cognition and Behaviour, Radboud University Nijmegen, Nijmegen, The Netherlands
[4]Interfaculty Institute for Genetics and Functional Genomics, University Medicine Greifswald, Greifswald, Germany
[5]Department of Psychiatry and Psychotherapy, HELIOS Hospital Stralsund, University Medicine Greifswald, Greifswald, Germany
[6]Department of Human Genetics, Radboud University Nijmegen Medical Center, Nijmegen, The Netherlands
[7]Department of Psychiatry, Donders Institute for Brain, Cognition and Behaviour, Radboud University Nijmegen Medical Center, Nijmegen, The Netherlands
[8]Department of Cognitive Neuroscience, Donders Institute for Brain, Cognition and Behaviour, Radboud University Nijmegen Medical Center, Nijmegen, The Netherlands
[9]Neurobiology of Language Department, Max Planck Institute for Psycholinguistics, Nijmegen, The Netherlands
[10]Institute of Diagnostic Radiology and Neuroradiology, University Medicine Greifswald, Germany
[11]Institute for Community Medicine, University Medicine Greifswald, Germany
[12]Donders Institute for Brain, Cognition & Behavior, Radboud University Nijmegen, Nijmegen, The Netherlands
[13]German Center for Neurodegenerative Diseases (DZNE), Site Rostock/Greifswald, Greifswald, Germany

---

Additional Supporting Information may be found in the online version of this article.

Conflict of Interest: No conflicts of interest are declared.

Contract grant sponsor: Biobanking and Biomolecular Resources Research Infrastructure, Netherlands (BBMRI-NL); Contract grant sponsor: Hersenstichting Nederland; Contract grant sponsor: Netherlands Organisation for Scientific Research (NWO); Contract grant sponsor: German Federal Ministry of Education and Research; Contract grant sponsor: German Ministry of Cultural Affairs; Contract grant sponsor: Social Ministry of the Federal State of Mecklenburg, West Pomerania; Contract grant sponsor: Siemens Healthcare, Erlangen, Germany; Contract grant sponsor: Federal State of Mecklenburg, West Pomerania.

*Correspondence to: Clyde Francks, Max Planck Institute for Psycholinguistics, Wundtlaan 1, Nijmegen 6525 XD, The Netherlands. E-mail: clyde.francks@mpi.nl

Received for publication 22 April 2013; Revised 29 July 2013; Accepted 26 August 2013.

DOI 10.1002/hbm.22401

Published online 4 November 2013 in Wiley Online Library (wileyonlinelibrary.com).

Abstract: Functional and anatomical asymmetries are prevalent features of the human brain, linked to gender, handedness, and cognition. However, little is known about the neurodevelopmental processes involved. In zebrafish, asymmetries arise in the diencephalon before extending within the central nervous system. We aimed to identify genes involved in the development of subtle, left-right volumetric asymmetries of human subcortical structures using large datasets. We first tested the feasibility of measuring left-right volume differences in such large-scale samples, as assessed by two automated methods of subcortical segmentation (FSL|FIRST and FreeSurfer), using data from 235 subjects who had undergone MRI twice. We tested the agreement between the first and second scan, and the agreement between the segmentation methods, for measures of bilateral volumes of six subcortical structures and the hippocampus, and their volumetric asymmetries. We also tested whether there were biases introduced by left-right differences in the regional atlases used by the methods, by analyzing left-right flipped images. While many bilateral volumes were measured well (scan-rescan $r = 0.6$–0.8), most asymmetries, with the exception of the caudate nucleus, showed lower repeatabilites. We meta-analyzed genome-wide association scan results for caudate nucleus asymmetry in a combined sample of 3,028 adult subjects but did not detect associations at genome-wide significance ($P < 5 \times 10^{-8}$). There was no enrichment of genetic association in genes involved in left-right patterning of the viscera. Our results provide important information for researchers who are currently aiming to carry out large-scale genome-wide studies of subcortical and hippocampal volumes, and their asymmetries. *Hum Brain Mapp 35:3277–3289, 2014.* © **2013 Wiley Periodicals, Inc.**

Key words: brain; lateralization; asymmetry; magnetic resonance imaging; genetics; genome-wide association scan; caudate nucleus; volumetry; subcortical

INTRODUCTION

A bilateral central nervous system (CNS) provides organisms with a basic organizing dimension that has resulted in differences between brain hemispheres in both function and anatomy [Ocklenburg and Gunturkun, 2012]. Although CNS asymmetries are found to different extents in arguably all vertebrates, and many invertebrates [Frasnelli et al., 2012], they seem to be pronounced in humans, where evidence points to subtle lateralization being a ubiquitous feature of brain structure and function [Toga and Thompson, 2003].

There has been much research linking neurodevelopmental disorders to departures from normal brain asymmetry, although such links have not been found in all clinical populations. Schizophrenia has been associated with patterns of reduced asymmetry [Berlim et al., 2003; Clark et al., 2010; DeLisi et al., 1997; Hayashi et al., 2012]. Language impairment and attention deficit hyperactivity disorder can also involve changes in asymmetric development of the brain [Boles and Barth, 2011; de Guibert et al., 2011; Schrimsher et al., 2002; Shaw et al., 2009]. While this evidence indicates an important role of lateralization in cognitive development, we still lack knowledge of the genetic mechanisms involved in patterning the normal asymmetries of the human brain, let alone the genetic variants that influence population variability in brain asymmetry.

The best studied animal model of CNS asymmetrical development is the zebrafish, in which early embryonic asymmetries within the diencephalon appear to act as precursors of broader brain asymmetries in subsequent development [Concha et al., 2009]. In particular, asymmetric formation of the zebrafish's epithalamus results in differential innervation of the two brain hemispheres, and contributes to their subsequent structural and functional divergence [Concha et al., 2009]. This process is linked to genetic and developmental mechanisms that give rise to left-right asymmetry of the viscera (e.g., heart forming to the left side; [Concha et al., 2000]). Furthermore, molecular asymmetries have been reported in the mouse hippocampus [Hou et al., 2013; Kawakami et al., 2003]. In humans, population-level volumetric asymmetries have been reported for the hippocampus, caudate nucleus, and thalamus [Alkonyi et al., 2010; Hou et al., 2013; Shi et al., 2009; Watkins et al., 2001; Yamashita et al., 2011]. Asymmetries in human subcortical structures and/or hippocampus may therefore play an important role as precursor to broader asymmetrical development of the human brain.

The goal of this study was to identify genetic loci that affect individual differences in subcortical and hippocampal asymmetries in humans, to shed light on the molecular mechanisms involved. We aimed to use genome-wide association scanning (GWAS) to link common polymorphisms to asymmetries of these structures in adult population samples. GWAS provides a relatively agnostic approach to finding novel genetic effects, and can thus generate new biological insights [Pearson and Manolio, 2008; Visscher et al., 2012]. In this study, our primary focus was on volumetric asymmetry, the relative difference in volume between the left (L) and right (R) sides of

these bilateral structures in the CNS, quantified as an asymmetry index (AI) according to the formula AI = 100 $(L - R)/(L + R)$. We were particularly interested in structures that showed a population-level asymmetry (i.e., mean AI significantly different from zero), as this would indicate genetically regulated mechanisms of asymmetrical development.

However, GWAS usually requires thousands of study participants pooled from multiple, heterogeneous sources, to yield sufficient statistical power to detect the effects of common DNA variants, in the context of massive multiple testing across the genome, and individual genetic effects that are anticipated to be small. This presents the challenge of assessing human brain asymmetry in large datasets from healthy, living subjects. Currently, this can only be achieved indirectly, through sophisticated imaging techniques, and automated methods of quantifying brain structure. Magnetic resonance imaging (MRI) and genome-wide genotyping of common single nucleotide polymorphisms (SNPs) are currently being used for such large-scale genetic studies of human brain structure [Stein et al., 2012].

Moreover, since we were interested in relatively small differences between left and right volumes, we anticipated the stability of individual difference measurement of AIs to be lower than for the absolute left or right volumes. For the purposes of genetic analysis, the repeatability of individual difference measurement in a quantitative phenotype sets an upper limit on the proportion of trait variance that can be attributed to heritable factors. If a large proportion of trait variance is likely to be due to measurement error, or other uncontrolled and nonreproducible factors that differ between MRI scans of the same subject, then the required sample sizes for genetic mapping must be accordingly larger. Therefore, we began by selecting candidate subcortical asymmetry traits for genetic analysis through detailed investigation of the measures produced by two widely used subcortical segmentation algorithms, FSL|FIRST and FreeSurfer [Fischl et al., 2002; Patenaude et al., 2011]. This analysis consisted of testing the robustness of measured asymmetries against methodological biases in left-right flipped brain images, and by analyzing the repeatability of variance in these measures across two MRI scans, taken at different time-points from the same set of subjects. In addition, we assessed the repeatability of the measures' residual variance, after correcting for covariates that are typically regressed out of brain imaging traits prior to GWAS. This would yield a more accurate representation of how repeatable the "variance of interest" is for genetic studies. In carrying out these analyses, we therefore extend the work done by Morey et al. on bilateral volumes [Morey et al., 2009, 2010], by testing the ability of the methods to measure variance in subtle left-right differences. Furthermore, we assessed the repeatability of individual difference measurement, which ultimately is the target of genetic analyses, for the bilateral volumes as well as their asymmetries.

We selected the most reliable asymmetry phenotype, that of the caudate nucleus, for GWAS with common polymorphisms in three large datasets, followed by genome-wide meta-analysis of association based on the data from all 3,028 subjects from the three datasets combined. Anatomically, each caudate nucleus (together with the putamen), receives several projections from the cortex. In turn, these project back to the cortex indirectly via the globus pallidus and thalamus [Draganski et al., 2008; Lehericy et al., 2004]. One role of the caudate nucleus has been hypothesized as gating information from the cortex, thus playing a role in cognitive control and behavior selection [Gil Robles et al., 2005; Grahn et al., 2008]. Consistent with this, there is functional evidence showing that the caudate nucleus subserves language processes such as bilingual lexical access [Crinion et al., 2006; Friederici, 2006]. Many language functions are relatively left-lateralized in the brains of most people [Knecht et al., 2000; Zatorre et al., 1992]. Previous studies have pointed to a rightward volume asymmetry of the caudate nucleus in humans, while reversed patterns of this asymmetry have been reported to associate with attention deficit symptoms in ADHD patients and healthy subjects, prenatal alcohol exposure, and schizophrenia [Qiu et al., 2009; Schrimsher et al., 2002; Uhlikova et al., 2007; Willford et al., 2010]. Therefore, identifying genetic effects on caudate nucleus asymmetry might provide insights into the aetiology of certain subtypes of common neuropsychiatric disorders.

MATERIALS AND METHODS

Participant Populations

The brain imaging genetics (BIG) study started in 2007 and is a collection of healthy volunteers, including many university students, who participated in studies at the Donders Centre for Cognitive Neuroimaging (DCCN), Nijmegen, The Netherlands [Franke et al., 2010]. At the time of this study, the BIG subject-pool consisted of 2,337 self-reported healthy individuals (1248 females), mean age 27.2 years (SD = 12.6), who had undergone anatomical (T1-weighted) MRI scans, usually as part of their involvement in diverse smaller-scale studies at the DCCN, and who had given their consent to participate in BIG. A subset of 235 subjects had undergone a brain MRI scan at least twice, with at least one day separation between scans. Fifty percent of the 235 rescans took place within 181 days of the first, with the mean elapsed time being 320 days (SD = 360). At the time of the first scan, their mean age was 24.2 (SD = 7.7). For the genetic analysis, genome-wide SNP genotype data were available from 1276 BIG subjects (see below for genotyping details). Their mean age was 22.9 (SD = 3.8) years, and 748 of these subjects were females.

The Study of Health in Pomerania (SHIP) is an ongoing, population-based study in northeast Germany,

aimed at describing the prevalence of common diseases and their risk factors. It now consists of two independent datasets: SHIP, and the more recently initiated SHIP-TREND. Participants had undergone a whole-body MRI scan, as well as genotyping for common polymorphisms. For more detailed information about the datasets [see Volzke et al., 2011]. For our genetic analyses, we were able to include 932 subjects from SHIP (491 females) with a mean age of 56.3 years (SD = 12.4) and 829 subjects from SHIP-TREND (461 females) with a mean age of 49.9 years (SD =13.4).

Image Acquisition

MRI data in BIG were acquired with either a 1.5 Tesla Siemens Sonata or Avanto scanner or a 3 Tesla Siemens Trio or TimTrio scanner (Siemens Medical Systems, Erlangen, Germany). Given that images were acquired during several smaller scale studies, the parameters used were slight variations of a standard T1-weighted three-dimensional magnetization prepared rapid gradient echo sequence (MPRAGE; 1.0 × 1.0 × 1.0 mm voxel size). The most common variations in the TR/TI/TE/saggital-slices parameters were the following: 2300/1100/3.03/192; 2730/1000/2.95/176; 2250/850/2.95/176; 2250/850/3.93/176; 2250/850/3.68/176; 2300/1100/3.03/192; 2300/1100/2.92/192; 2300/1100/2.96/192; 2300/1100/2.99/192; 1940/1100/3.93/176; and 1960/1100/4.58/176. There was also variation in the number of headcoils used across BIG scans, with the following arrays being employed (and their frequencies): 32-channel (26%), 12-channel (5%), 8-channel arrays (32%), and single headcoil (37%).

For the GWAS sample, 634 subjects were scanned at 1.5 T, and 642 subjects at 3 T. Of the 235 double-scanned subjects, 30 were scanned twice at 1.5 T, 70 subjects twice at 3 T, and 135 subjects were scanned at both field strengths.

For the SHIP datasets, all MRI images were obtained on a 1.5 T scanner (Magnetom Avanto; Siemens Medical Systems, Erlangen, Germany), using a standard T1-weighted MPRAGE sequence (TE 1900.0, TR 3.4, Flip angle 15°, 1.0 × 1.0 × 1.0 mm voxel size; Hegenscheid et al., 2009).

Segmentation and Derivation of Measures

A default correction was applied against field inhomogeneities, implemented in the Siemens scanners we employed. In addition, segmentation with FreeSurfer included a bias field correction step. The orientation of the images was extracted directly from the DICOM files, which were then converted into nifti format using SPM5's "spm_dicom_convert" function. To preserve the correct left-right orientation for all subsequent steps, all images were first reoriented to the MNI152 standard using FSL's (version 4.1) "fslreorient2std" function. FSL|FIRST (version 1.2) segmentation parameters were set according to the ENIGMA (Enhancing Neuro-Imaging Genetics Through Meta-Analysis) protocol, (http://enigma.loni.ucla.edu/protocols/imaging-protocols/), and are listed in Supporting Information Table I. FreeSurfer subcortical segmentations were produced with the standard "-recon-all" processing pipeline and default parameters. From these analyses, we extracted left (L) and right (R) volumes of seven paired, bilateral structures; amygdala, nucleus accumbens, caudate nucleus, globus pallidus, putamen, thalamus, and hippocampus (see Fig. 1 for an example comparison of both segmentation procedures). For each structure, percentage differences between the left and right volumes were expressed as an AI, calculated by the formula AI = 100 × $(L - R)/(L + R)$, whose values could range theoretically from −100 to +100, with positive values denoting a larger left structure, negative values a larger right structure, and zero in the case of perfect volume symmetry. Estimates of total brain volume (TBV) were calculated as the voxel-wise sum of the gray matter and white matter probability maps produced by the VBM5.1 toolbox, version 1.19 (http://dbm.neuro.uni-jena.de/vbm/), in SPM5 and with default settings. Exclusion of outlier values (more extreme than 3.5 SD from the mean), correction for covariates and residual extraction, was done with MS Excel (2010) using VBA scripting. In

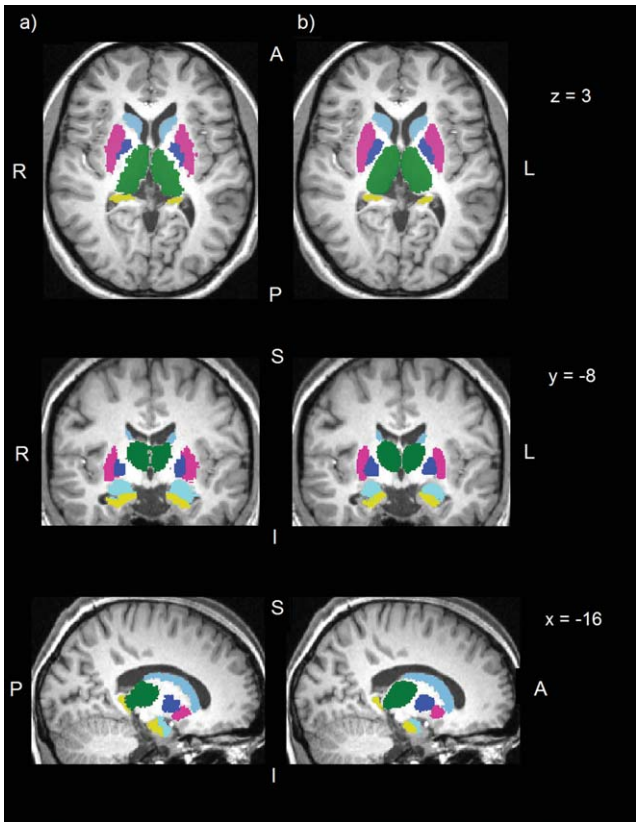

Figure 1.
Example segmentation of subcortical structures. The two columns show the segmentation results of the same (normalized) brain by (**a**) FreeSurfer and (**b**) FSL|FIRST in three different slices.

line with imaging genetic association studies [Stein et al., 2012; http://enigma.loni.ucla.edu/protocols/genetics-protocols/], the following covariates were controlled for in subsequent analyses: gender, age, TBV, and field strength (the latter only in BIG). Note that we did not include handedness as a covariate effect on AIs because handedness itself is a partly heritable trait [Medland et al., 2009]. Therefore, any shared variance of AIs with handedness was important to retain for genetic analysis.

Left-Right Flipped Image Analysis

In simple terms, segmentations done by both FSL|FIRST and FreeSurfer rely on defining structures in the brain while using prior knowledge (probability maps) from sets of manually segmented reference images. To test for possible influences of asymmetries in these probability maps, we randomly selected a subset of 44 BIG subjects and flipped their image data on the left-right axis (without changing the image header), so that the left sided structures would then be segmented according to the software's definition of the right side, and vice versa.

Repeatability Analysis

For each structure, we used data from 235 twice-scanned subjects to assess the scan-rescan correlations for the measures of bilateral, summed volumes ($L + R$), and the AIs. We also analyzed the agreement between FSL|FIRST and FreeSurfer outputs for these measures. We employed Pearson correlations to measure the amount of phenotypic variance common to both scan sessions/segmentation methods. In addition, we also included calculations of intraclass correlations (ICC) using two-way mixed effects models [McGraw and Wong, 1996; Shrout and Fleiss, 1979], to allow a more direct comparison of our results with previous work on segmentation accuracy. These analyses were done in IBM SPSS (v. 20).

Genotyping

Genotyping of BIG was performed using the Affymetrix Genome-Wide Human SNP Array 6.0 (Affymetrix, Santa Clara, CA). Genotype calls were made using the Birdseed algorithm [Rabbee and Speed, 2006]. Samples were excluded that had call rates <90% and that showed deviant values of genome-wide heterozygosity [Purcell et al., 2007], as this can indicate the presence of genotyping artifacts. SNPs with a minor allele frequency below 1% or that failed the Hardy-Weinberg equilibrium test at a threshold of $P \leq 10^{-6}$ were also excluded [Purcell et al., 2007]. The resulting markers were then adjusted to the forward strand, as to avoid any ambiguity problems in subsequent steps. A 2-step imputation protocol was followed, to use the genotyped set of markers to infer the genotypes at millions of additional positions in the human genome. We used the software MACH for haplotype phasing and minimac for the final imputation [Howie et al., 2012; Li et al., 2010], with the 1,000 Genomes Phase 1.v3 EUR reference panel [The 1000 Genomes Project Consortium, 2010]. All monomorphic markers were removed from the reference dataset. Individual genotype calls that had an imputation certainty <90% were removed, as were markers with an overall quality score below 0.3 R^2. As a final quality filter, only markers with no more than 5% missing data were selected. At the end of these procedures, genotypes were available for 1,276 subjects from BIG, for 6,131,824 SNPs spanning the genome.

Genotyping of the SHIP and SHIP-TREND samples was done on two different platforms, the Affymetrix Genome-Wide Human SNP Array 6.0 and Illumina Human Omni 2.5, respectively. In SHIP, the genotype calling was performed with the Birdseed algorithm and samples were excluded with call rates <86%. For SHIP-TREND, calls were done on the GenomeStudio Genotyping Module v1.0, and excluded samples had a call rate <94%. For both samples, markers that failed Hardy-Weinberg equilibrium ($P < 10^{-4}$) were removed, as well as markers that had more than 20 and 10% missing data in SHIP and SHIP-TREND, respectively. Imputation of nonobserved genotypes was performed on both samples separately, but with the same protocol. The reference panel used, as for the BIG sample, was an all polymorphic 1000 Genomes Phase 1.v3 EUR panel [The 1000 Genomes Project Consortium, 2010]. A two-step approach was used, performed with the software IMPUTE v2.1.2.3 [Howie et al., 2009]. This resulted in genotypes for 17,533,349 markers in 932 subjects for SHIP and 17,585,496 markers in 829 subjects for SHIP-TREND.

GWAS for Asymmetry of the Caudate Nucleus

We carried out GWAS using the Caudate Nucleus AI as a quantitative phenotype, in each of the three datasets separately. The following covariates were controlled for in all three datasets: age, gender, and TBV. In addition, scanner field strength was controlled for in BIG (at either 1.5 or 3 T). The association tests were performed using linear regression, as implemented in PLINK v1.07 [Purcell et al., 2007].

GWAS Meta-Analysis

The GWAS results from the three datasets were merged using the "sample size" approach in the software METAL [Willer et al., 2010]. Put briefly, this approach pools the probabilities of a genetic effect at each SNP, across the three contributing studies, and weighted by each study's sample size, while considering the direction of the allelic effect on the quantitative trait. We chose this method because our three populations differed in terms of mean age and other aspects of their recruitment, so that we wished to avoid assuming an equivalence of genetic effect

sizes across them. Finally, we considered only results from SNPs that were present in each of the three datasets, resulting in 4,187,195 markers genome-wide.

Genetic Candidate Pathway Analysis

We tested for an enrichment of association between asymmetry of the caudate nucleus and genes involved in left-right visceral determination, using the software INRICH [Lee et al., 2012]. Briefly, this approach identifies distinct regions of linkage disequilibrium (LD) in the genome that show association with a trait of interest, below a certain threshold of nominal significance. The regions of LD are mapped to genes, which are assigned to defined biological pathways, processes or groups according to prior gene-functional data. Then, regions of LD are shuffled across genes by permutation, to arrive at an empirical measurement of how often the real-data pattern of association within pathways would be observed by chance alone. This approach is robust to the effect that a gene's or pathway's genomic size has on its probability of containing nominally significant associations. We used the default parameters, with the exception of the following: the flanking regions, for a gene to be considered hit by an interval, were $+/-100$ kb, and pathways had to consist of 10 or more genes to enter the analysis.

We used the GWAS meta-analysis as our source of nominal P values ($P \leq 0.001$), in order that our analysis would be maximally powered. A practical constraint that arose from this approach was that we needed to use the LD structure from only one of the datasets (we chose BIG), but there is no reason to expect substantial differences in the genomic distribution of LD between the Dutch and Northern German populations. We used the Gene Ontology (GO; [Ashburner et al., 2000]) as our source of assignments of genes to biological pathways. We searched the GO annotation file provided with INRICH for pathways involved in visceral left-right asymmetry determination, using the search terms "symmetry," "asymmetry," "left," "right," and "left/right." Six relevant pathways were found, of which one fulfilled the size criterion for association enrichment testing. This pathway was "Determination of left/right symmetry."

RESULTS

Volume Measures

Table I shows the volume measurements and AIs in the three studies, before adjustment for the covariate effects of age, gender, TBV, and field strength (the latter only in BIG). A more detailed depiction of the distribution of volumes and AIs in the three studies can be found in Supporting Information Figure S1 and S2. The segmentations of the BIG sample resulted in volumes that were larger than those observed in the SHIP datasets (Table I). Taken across all structures together, BIG volumes were 10.6% larger for FSL|FIRST segmentations and 13.3% larger for FreeSurfer, than in SHIP and SHIP-TREND. To investigate whether the differences in age between BIG and SHIP could explain this observed difference in volumes, we modeled the effect of age on GM and TBV within the BIG sample (Supporting Information Fig. S3). We observed linear decreases of GM and TBV with increased age that resulted in a volumetric reduction of 15% (GM) and 8% (TBV) between the ages of 27 and 53, which are the mean ages of the BIG and SHIP datasets, respectively.

There were notable differences between FSL|FIRST and FreeSurfer in the mean measurements of volumes of some structures. FreeSurfer measures, relative to FSL|FIRST, were greater for the amygdala (19% larger), nucleus accumbens (9% larger), hippocampus (7% larger), and putamen (5% larger). FSL|FIRST yielded greater measures for the globus pallidus (8% larger) and thalamus (7% larger), relative to FreeSurfer.

Almost all structures showed mean AIs that were significantly different from zero for both segmentation methods, with the exception of the amygdala, as segmented by FSL|FIRST, in SHIP and SHIP-TREND (Table I). The most pronounced deviations from mean AI = 0 were observed for the thalamus and nucleus accumbens for the FSL|FIRST segmentations, and for the putamen and globus pallidus for FreeSurfer. These asymmetries were particularly striking, with the mean AI's roughly 1 standard deviation from zero. In the case of the FSL|FIRST measurement of the thalamus, for example, this corresponded to the left structure being assessed 2.5% larger on average than the right.

For each separate structure and method, the direction of the mean shift from AI = 0 was largely concordant across the three datasets, with the exception of the FreeSurfer measurements of the nucleus accumbens. For this measure, the BIG sample showed the opposite mean shift of AI, relative to SHIP and SHIP-TREND. Discordances between FSL|FIRST and FreeSurfer, in terms of the direction of mean shifts from AI = 0, were seen for the thalamus (positive AI with FSL|FIRST in all three studies, and negative AI with FreeSurfer in all three studies), and globus pallidus (negative AI with FSL|FIRST in all three studies, and positive AI with FreeSurfer in all three datasets; Table I).

Flipped Image Analysis

Forty-four subjects randomly drawn from BIG were analyzed both before and after left-right flipping of their input images into segmentation. As expected, the "un-flipped" AI means for these 44 subjects (Table II) were representative of those for the whole BIG dataset (2,337 subjects; Table I), although not all AIs showed a statistically significant mean shift from 0 in this relatively small subset (Table II). The mean shift from zero of the AI was reversed

TABLE I. Means and standard deviations for L and R volumes (in mm^3) and AIs, derived from FSL|FIRST and FreeSurfer in the three study datasets, before correction for covariate effects, and standardization

		FSL|FIRST			FreeSurfer		
		BIG	SHIP	SHIP-T	BIG	SHIP	SHIP-T
Nucleus Accumbens	*L*	572.5 (117.4)	493.1 (116.5)	516.6 (109.2)	582.4 (120.0)	488.1 (82.2)	498.9 (83.5)
	R	486.1 (109.1)	395 (101)	424.6 (93.1)	622.8 (117.5)	432.9 (80.1)	445.2 (85.4)
	AI	8.4[a] (8.7)	11.2[a] (10.2)	9.8[a] (8.5)	−3.4[a] (8.7)	6.1[a] (7.6)	5.9[a] (7.8)
Amygdala	*L*	1377.2 (245.8)	1208.3 (215)	1222.3 (202.4)	1581.5 (222.6)	1441.6 (183.4)	1457.9 (183.6)
	R	1375.5 (283.1)	1212.8 (237)	1225.8 (226.5)	1608.0 (212.9)	1518.9 (193.6)	1534.6 (193.7)
	AI	−0.6[b] (9.7)	0.0 (8.9)	0.1 (8.2)	−0.9[a] (4.4)	−2.6[a] (4.2)	−2.6[a] (4.2)
Caudate Nucleus	*L*	3786.0 (457.0)	3343.7 (405.5)	3383.7 (407.7)	3881.6 (515.8)	3547.5 (470.5)	3582.3 (468.7)
	R	3879.1 (485.0)	3403.1 (408.9)	3441.7 (412.8)	3926.1 (526.3)	3593.3 (487.1)	3622.6 (481.2)
	AI	−1.3[a] (2.3)	−0.9[a] (2.7)	−0.9[a] (2.4)	−0.6[a] (2.2)	−0.6[a] (2.4)	−0.6[a] (2.3)
Hippocampus	*L*	3936.8 (446.7)	3681.3 (436.7	3715.2 (438.2)	4338.4 (457.3)	3834.0 (445.4)	3892.3 (437.7)
	R	3971.5 (460.9)	3807.3 (440.1)	3818.6 (422.5)	4380.5 (467.6)	3930.1 (465.1)	3977.0 (445.1)
	AI	−0.5[a] (4.8)	−1.7[a] (4.4)	−1.4[a] (4.3)	−0.5[a] (2.8)	−1.2[a] (3.0)	−1.1[a] (2.9)
Globus pallidus	*L*	1821.6 (191.6)	1708.4 (223.3)	1709.5 (202.4)	1844.0 (261.9)	1614.5 (232.8)	1643.5 (234.1)
	R	1847.4 (188.4)	1744.3 (219.4)	1743.5 (202.1)	1658.2 (235.4)	1465.2 (220.3)	1496.9 (225.0)
	AI	−0.7[a] (3.4)	−1.1[a] (3.9)	−1.0[a] (3.9)	5.2[a] (4.6)	4.9[a] (4.5)	4.7[a] (4.6)
Putamen	*L*	5276.2 (583.6)	4816 (599.66)	4876.9 (588.2)	5812.1 (720.0)	4932.3 (652.1)	4993.9 (671.8)
	R	5286.8 (585.4)	4748.2 (578.3)	4796.8 (575.3)	5538.5 (694.1)	4766.2 (636.9)	4824.5 (652.3)
	AI	−0.1[b] (2.6)	0.7[a] (2.9)	0.8[a] (2.8)	2.4[a] (2.1)	1.7[a] (2.6)	1.7[a] (2.7)
Thalamus	*L*	8437.3 (779.8)	7554.2 (802.1)	7680.5 (836.5)	7607.2 (933.2)	6990.5 (887.9)	7139.2 (942.1)
	R	8242.5 (772.4)	7357 (803.8)	7478.0 (818.3)	7718.7 (942.2)	7205.7 (936.9)	7369.8 (981.2)
	AI	1.2[a] (1.6)	1.3[a] (1.7)	1.3[a] (1.7)	−0.8[a] (2.8)	−1.5[a] (2.7)	−1.6[a] (2.8)
N		2330	1057	1905	2330	1120	2092

Mean AI is significantly different from 0.
[a]$P < 0.005$.
[b]$P < 0.05$.

or cancelled in the flipped images, compared with nonflipped images, for the caudate nucleus as segmented by FSL|FIRST, and for the amygdala, caudate nucleus, globus pallidus, and thalamus as segmented by FreeSurfer (Table II). Other structures including the nucleus accumbens (for the FSL|FIRST and FreeSurfer segmentations) and the thalamus (for the FSL|FIRST segmentation) failed to reverse the direction of their mean AI shift from zero in flipped images, as compared with nonflipped images (Table II).

TABLE II. Means and standard deviations of AIs in a subset of 44 BIG subjects, for both the original and left-right flipped images

	FSL|FIRST		FreeSurfer	
	Original	Mirrored	Original	Mirrored
Nucleus Accumbens	8.0 (9.5)[a]	5.8 (10.4)[a]	−2.4 (6.5)[a]	−7.7 (6.0)[a]
Amygdala	0.2 (9.0)	−0.7 (13.0)	**−1.8 (3.9)**[a]	**1.9 (4.6)**[a]
Caudate Nucleus	**−0.9 (2.1)**[a]	**2.0 (2.9)**[a]	**−0.8 (2.3)**[a]	**0.2 (2.1)**
Hippocampus	0.5 (3.9)	−1.6 (4.3)[a]	0.1 (2.6)	1.0 (2.6)[a]
Globus pallidus	−0.4 (3.5)	−1.6 (2.9)[a]	**5.4 (4.1)**[a]	**−0.2 (5.2)**
Putamen	0.0 (2.4)	1.0 (2.6)[a]	2.6 (1.9)[a]	2.0 (1.9)[a]
Thalamus	1.3 (1.4)[a]	2.3 (1.7)[a]	**−1.0 (2.4)**[a]	**1.9 (2.2)**[a]

In bold are the values that show an appropriate sign change when input images were flipped.
[a]Mean AI is significantly different from 0 at $P < 0.05$.

Repeatability Analysis

Within the 235 BIG subjects who had been scanned twice, we used Pearson correlations to assess the agreement between the first and second scans for bilateral volumes ($L + R$), as well as the residual bilateral volumes after correcting for the covariate effects (Table III). These covariate effects are typically regressed out prior to genetic analysis of brain volumetric measures [Stein et al., 2012] and results of these regressions can be found in Supporting Information Table II. Overall, there was a decrease in scan-rescan correlations for the residuals, as compared with the unadjusted volumes, for both FSL|FIRST and FreeSurfer (Table III). This was particularly pronounced for the thalamus as segmented by FSL|FIRST, for which the scan-rescan correlation dropped from 0.907 (unadjusted bilateral volume) to 0.664 (adjusted bilateral volume), meaning that 44% of the variance in this residualized measure was shared between first and second scan. For FreeSurfer measures of bilateral volumes, four of

TABLE III. Repeatability (Pearson *r* between first and second MRI scan measures), based on 235 BIG subjects, for summed bilateral volumes (*L* + *R*), before and after adjustment for covariate effects of gender, age, TBV, and field strength

	FSL|FIRST		FreeSurfer	
	Raw volumes	Adjusted volumes	Raw volumes	Adjusted volumes
Nucleus Accumbens	0.685[a]	0.670[a]	0.639[a]	0.546[a]
Amygdala	0.574[a]	0.650[a]	0.714[a]	0.559[a]
Caudate Nucleus	0.944[a]	0.798[a]	0.926[a]	0.810[a]
Hippocampus	0.873[a]	0.795[a]	0.775[a]	0.645[a]
Globus pallidus	0.862[a]	0.693[a]	0.717[a]	0.589[a]
Putamen	0.898[a]	0.774[a]	0.873[a]	0.717[a]
Thalamus	0.907[a]	0.664[a]	0.774[a]	0.555[a]

[a]Significance of the correlation $P < 0.005$.

the structures (nucleus accumbens, amygdala, globus pallidus, and thalamus) showed scan-rescan correlations that were <0.6, after adjustment for covariate effects. This means that less than 36% of the variance in these residualized measures was shared between first and second scans. When subjects were scanned twice using the same scanner (either 1.5 or 3 T) the repeatabilities were slightly higher than when subjects were scanned once at 1.5 and once at 3 T. However, we did not have sufficient power to test the significance of these subtle differences in within-scanner and between-scanner correlation coefficients (see Supporting Information Table III).

We also used the 235 twice-scanned BIG subjects to correlate the AIs between the first and second scans for each structure, as well as the residual, standardized AIs after adjusting for the covariate effects (Table IV). Overall, the scan-rescan correlations for AIs (Table IV; See Supporting Information Figs. S4 and S5 for plots of these correlations) were lower than those for the bilateral volumes. Nonetheless, the AIs of the caudate nucleus, hippocampus, and thalamus, as segmented with FSL|FIRST, showed scan-rescan correlations higher than 0.6 (Table IV). None of the FreeSurfer AIs showed scan-rescan correlations >0.5 (Table IV). In addition, we also tested the absolute agreement of bilateral volumes (*L* + *R*) and AI's, between the first and second scans, using ICC, results of this analysis can be seen in Supporting Information Table IV.

TABLE IV. Repeatability (Pearson *r* between first and second MRI scan measures), based on 235 BIG subjects, for AIs, before and after adjustment for covariate effects of gender, age, TBV, and field strength

	FSL|FIRST		FreeSurfer	
	Raw AI	Adjusted AI	Raw AI	Adjusted AI
Nucleus Accumbens	0.570[a]	0.570[a]	0.260[a]	0.350[a]
Amygdala	0.570[a]	0.542[a]	0.370[a]	0.398[a]
Caudate Nucleus	0.647[a]	0.652[a]	0.441[a]	0.454[a]
Hippocampus	0.632[a]	0.626[a]	0.507[a]	0.482[a]
Globus pallidus	0.562[a]	0.560[a]	0.088	0.091
Putamen	0.446[a]	0.528[a]	0.291[a]	0.313[a]
Thalamus	0.614[a]	0.609[a]	0.183[a]	0.188[a]

[a]Significance of the correlation $P < 0.005$.

TABLE V. Agreement between FSL-FIRST and FreeSurfer (Pearson *r*), based on 235 BIG subjects, for summed bilateral volumes (*L* + *R*), and AIs [100 (*L* − *R*)/(*L* × *R*)], before and after adjustment for covariate effects of gender, age, TBV, and field strength

		FSL|FIRST and FreeSurfer		
	Raw Volumes	Adjusted volumes	Raw AI	Adjusted AI
Nucleus Accumbens	0.377[a]	0.327[a]	0.090	0.165[b]
Amygdala	0.177[a]	0.125	0.094	0.113
Caudate Nucleus	0.894[a]	0.855[a]	0.357[a]	0.392[a]
Hippocampus	0.692[a]	0.609[a]	0.217[a]	0.210[a]
Globus pallidus	0.688[a]	0.529[a]	0.119	0.127
Putamen	0.785[a]	0.668[a]	0.094	0.122
Thalamus	0.764[a]	0.501[a]	−0.011	0.009

[a]Significance of the correlation $P < 0.005$.
[b]Significance of the correlation $P < 0.05$.

Correlations Between Measures Derived from FSL|FIRST and FreeSurfer

Using only data from the first scan of the 235 twice-scanned BIG subjects, we assessed the agreement between FSL|FIRST and FreeSurfer in terms of measuring individual differences in bilateral volumes and AIs for each structure, both before and after adjustment for covariate effects (Table V). The bilateral volume of the caudate nucleus stood out as being reliably measured across the two methods ($r = 0.855$ after adjustment for covariates), while the bilateral volumes of the hippocampus and putamen also showed intermethod correlations >0.6 after adjustment for covariate effects (Table V). The AIs generally showed low agreement between FSL|FIRST and FreeSurfer (Table V; Supporting Information Fig. S6), with the caudate nucleus AI proving to be the most consistent between the two methods ($r = 0.392$ after adjustment for covariates). The same pattern of results is also found when assessing ICC of consistency, between FSL|FIRST and FreeSurfer, for measures of bilateral volumes and AI's (see Supporting Information Table V).

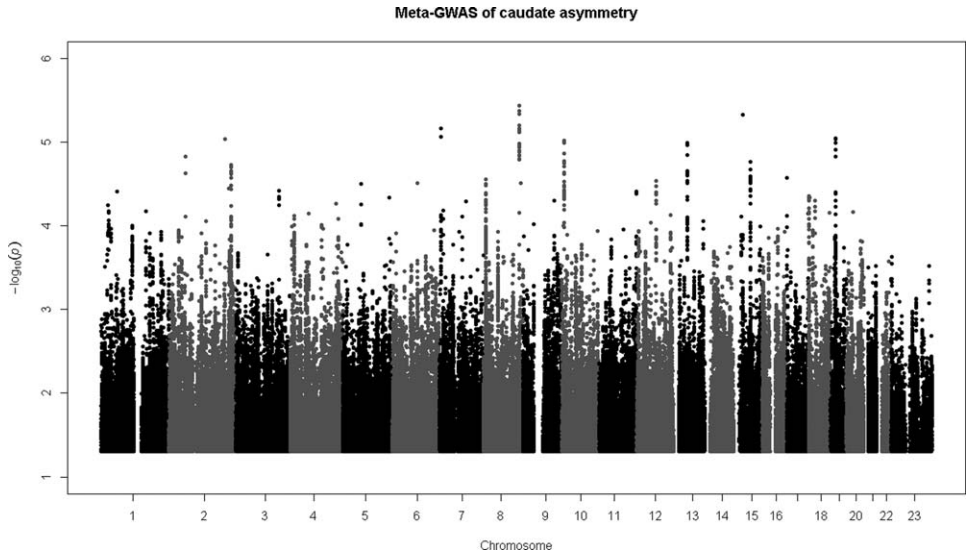

Figure 2.

Meta-GWAS of caudate nucleus asymmetry (FSL|FIRST). The X-axis represents each of the chromosomes arranged from end-to-end, from p arm to q arm, in ascending numerical order from left to right. The Y-axis represents the pointwise significance of association with caudate AI (Plotted only nominal $P < 0.05$). Colors and shades distinguish SNPs from different chromosomes.

Genetic Analysis

GWAS meta-analysis of the caudate nucleus AI (FSL|FIRST), for which we merged genetic association data across the three study datasets for each of 4,187,195 SNPs spanning the genome, did not identify an individual association that surpassed the commonly applied significance threshold for GWAS of $P = 5 \times 10^{-8}$ (Fig. 2). The most significant individual locus was rs75553296 ($P = 1.4 \times 10^{-6}$) on chromosome 16q32.1, which is 80 kilobases upstream of the gene NUDT7. This gene encodes a protein member of the Nudix hydrolase family, which eliminates potentially toxic nucleotide metabolites from the cell, and regulates the concentrations and availability of many different nucleotide substrates, cofactors, and signaling molecules (provided by RefSeq; http://www.ncbi.nlm.nih.gov/nuccore/343887371).

There was no significant enrichment of association within genes involved in visceral left-right axis determination. Of the 36 genes assigned to this GO pathway, none individually contained SNPs that showed association with the caudate nucleus AI at nominal $P < 0.001$.

DISCUSSION

Automated methods of segmenting brain structures from T1-weighted MRI images are currently the most feasible option for performing large scale, genome-wide association analysis of human brain morphology. Such analysis requires thousands of participants and in practice must usually be based on pooled data, or meta-analyzed data, from multiple, separate sources. GWAS studies of subcortical and hippocampal volumes, and their volumetric asymmetries, are already underway [Bis et al., 2012; Renteria et al., 2011, 2012; Sleiman et al., 2012; Stein et al., 2012]. In this study, we performed an investigation of candidate phenotypes for large-scale genetic studies of subcortical and hippocampal volumes and their asymmetries, evaluating results from two widely used segmentation software packages. Our results can contribute to on-going, consortium-based genetic studies, as regards the choices of measures to be pursued for genetic analysis, and/or the interpretation of genetic findings that arise for particular measures.

The mean volume measurements for various structures differed between our study datasets, and between segmentation methods. We showed that the larger volumes measured in the BIG dataset, as compared to the SHIP datasets, were as expected given the average ages of the different collections [Good et al., 2001; Sherwood et al., 2011]. However, we cannot exclude the possibility that other, uncontrolled differences in study protocol or image acquisition may also have had minor contributions to the differences in mean volumes between the datasets.

The mean volume differences between the two segmentation methods, for example for the hippocampus (larger with FreeSurfer) and thalamus (larger with FSL), are likely

to have arisen from differences in the anatomical definitions of the regions in the probability maps used by the two programs, as well as from differences in the segmentation algorithms, including differences in the weighting of the prior probability maps [Fischl et al., 2002; Patenaude et al., 2011].

Regardless of systematic differences in mean volume measurements between studies and segmentation methods, it is important to note that, for the purposes of genetic analysis, the focus is on the relative individual differences between subjects, and how accurately these can be determined. Therefore, our focus for repeatability analysis, either using double-scanned subjects to evaluate the segmentation methods, or for comparing the two segmentation methods against each other, was on the correlation of measured variance, and not on the accuracy of mean volume measurement.

For bilateral volumes ($L + R$), which are currently the focus of consortium GWAS in tens of thousands of subjects [Bis et al., 2012; Ikram et al., 2012; Stein et al., 2012], our data showed good repeatability across scans for the larger volumes in the uncorrected analysis, although repeatability was somewhat reduced after adjustment for the covariate effects of gender, age, TBV, and scanner field strength. For many structures, with either segmentation method, scan-rescan correlations of covariate-adjusted bilateral volumes were <0.7, which corresponds to 49% of trait variance being shared from first to second scan. The heritable proportion of variance in these measures is likely to be lower. Our results clearly underscore the necessity of meta-analyzing data from thousands of individuals to obtain sufficient power for GWAS studies of these traits. Before correction for covariate effects, the repeatabilities of bilateral volume measurements were comparable, but slightly lower, than those reported previously in smaller samples [Morey et al., 2009, 2010]. This is likely to be due to our use of a more heterogeneous sample in terms of scanning parameters, which have been previously found to have a subtle effect on the repeatability of volumetric measurements [Wonderlick et al., 2009]. Our finding of a greater reliability for segmentation of larger structures compared to smaller ones is in agreement with previous reports [Nugent et al., 2012; Wonderlick et al., 2009].

For AIs, which are also now beginning to be investigated in the context of genetic mapping [Renteria et al., 2011], the first step was to identify structures for which we could reliably detect a population-level bias in the direction of their asymmetry, as this would suggest the presence of regulated genetic/developmental mechanisms in generating such a bias. While several structures seemed to show population-level asymmetry at face value (i.e., having a mean AI that differed significantly from zero), not all structures were consistent between the two segmentation methods in the direction of this mean shift, and some failed to show a reversed mean shift after left-right flipping of the T1 images. Together, these observations indicate that, for some structures, the methods were affected by different asymmetries that existed in their prior probability maps. One possibility is that there was not always enough tissue contrast in the input images to define some structures clearly [Nugent et al., 2012]. Another possibility, that has not been investigated to our knowledge, is that subtle differences in shape between the left- and right-sided structures did not allow proper segmentation of left-right flipped images. In either case, the segmentations would ultimately be weighted more on the algorithms' prior information. The algorithms both rely on atlases constructed from manual segmentations (considered the gold standard), and there is in fact evidence of systematic left-right bias in manual segmentations [Maltbie et al., 2012]. The caudate nucleus stood out as the only structure showing a reversed mean shift of AI in the flipped images for both segmentation methods, as well as a close agreement between methods in the direction and magnitude of mean AI. This made us confident that the mean left-right asymmetry of the caudate nucleus was driven mostly by the images, and not by the prior probability maps for this structure, and that the caudate nucleus therefore showed a real population-level asymmetry in our study datasets.

For all structures, the scan-rescan correlations of AIs were lower than those for summed, bilateral volumes ($L + R$). This was not surprising, as the volumetric differences between left and right sides were equivalent to only small proportions of the structures' overall volumes. Clearly, the repeatability of AI individual difference measurement is dependent on the presence of true and variable asymmetries in the images. Poor repeatability of AIs may arise when individual differences are very subtle, in which case the AIs will predominantly reflect error variance. The scan-rescan analysis again supported the caudate nucleus as showing the most robustly assessed asymmetry. This structure had the highest scan-rescan correlations for raw and covariate-adjusted volumes, regardless of the segmentation method. Furthermore, in the correlation analysis of measures produced by FSL|FIRST with those produced by FreeSurfer, it was again the caudate nucleus that showed the best agreement between the two methods, for bilateral volumes and AIs. This is in agreement with the results of [Wonderlick et al., 2009], where the measures of caudate volume also showed robustness against variability in image acquisition. This is likely due to the caudate showing clear tissue contrasts with the neighboring white matter and cerebrospinal fluid.

In general, FSL|FIRST showed slightly higher scan-rescan correlations than FreeSurfer, both for bilateral volumes and AIs (and the covariate-adjusted residuals derived from them). It is difficult to draw general conclusions from our study on the relative merits of FSL|FIRST and FreeSurfer for supporting genetic analysis of subcortical structures, as the heterogeneity of scan acquisition parameters in the 235 twice-scanned subjects from BIG may have affected the two methods' performance in different ways. However, this heterogeneity was a valid representation of the reality that is

commonly encountered in pooled datasets for large-scale genetic association studies, which require thousands of participants from multiple sources [Stein et al., 2012]. Our data are therefore informative in this "real-world" context.

We are already contributing data from the BIG and SHIP datasets to consortium GWAS analysis of bilateral subcortical volumes, which will be reported elsewhere. Here, we focused on genetic analysis of the most reliably measured subcortical asymmetry in our datasets, that of the caudate nucleus. The fact that the caudate nucleus showed a consistent, population-level asymmetry in all studies, and with both segmentation algorithms, which also reversed correctly in flipped images, suggests strongly that caudate nucleus asymmetry is real and that at least part of this trait is genetically regulated. Our GWAS meta-analysis of caudate nucleus AI (FSL-FIRST), based on 3,028 subjects, resulted in no marker reaching statistical significance. We conclude that GWAS meta-analysis of more datasets will be required to detect individually significant genetic effects on this trait. We found no evidence from our genetic pathway analysis that genes involved in left-right visceral axis determination affect caudate nucleus asymmetry. However, although the caudate nucleus AI was the most reliably measured asymmetry, there was only a modest agreement between FSL-FIRST and FreeSurfer in terms of measuring the individual differences between subjects. This suggests that disagreements in the exact neuroanatomical definitions of the structure exist within the atlases used by the two methods, which can only be resolved through detailed neuroanatomical investigation.

To conclude, GWAS studies of quantitative traits in the general population usually assume that many common genetic variants will each have small individual contributions. The statistical correction needed, to account for multiple testing across the whole genome, results in having to gather large numbers of subjects (in the thousands) to achieve reasonable statistical power. Brain imaging genetics is a growing field that will depend crucially on automated methods of image segmentation and analysis. In this article, we highlight the importance of careful, prior assessment of trait properties and reproducibility for such large scale studies. Our findings can contribute to future research on subcortical and hippocampal volumes and their asymmetries, and indicate in particular that the caudate nucleus is a promising structure to investigate further in this context, with larger sample sizes.

ACKNOWLEDGMENTS

This work makes use of the BIG (Brain Imaging Genetics) database, first established in Nijmegen in 2007. This resource is now part of Cognomics, a joint initiative by researchers of the Donders Centre for Cognitive Neuroimaging, the Human Genetics and Cognitive Neuroscience departments of the Radboud University Medical Centre and the Max Planck Institute for Psycholinguistics. The Cognomics Initiative is supported by the participating departments and centres. The authors wish to thank all persons who kindly participated in this research. The SHIP datasets are part of the Community Medicine Research net (CMR) of the University of Greifswald. Genome-wide data and MRI scans were supported by the Federal Ministry of Education and Research. The University of Greifswald is a member of the Center of Knowledge Interchange program of the Siemens AG and the Caché Campus Program of the InterSystems GmbH. The SHIP authors are grateful to Mario Stanke for the opportunity to use his Server Cluster for the SNP imputation.

REFERENCES

Alkonyi B, Juhasz C, Muzik O, Behen ME, Jeong J-W, Chugani HT (2010): Thalamocortical connectivity in healthy children: Asymmetries and robust developmental changes between ages 8 and 17 years. AJNR Am J Neuroradiol 32:962–969.

Ashburner M, Ball CA, Blake JA, Botstein D, Butler H, Cherry JM, Davis AP, Dolinski K, Dwight SS, Eppig JT, et al. (2000): Gene ontology: Tool for the unification of biology. The gene ontology consortium. Nat Genet 25:25–29.

Berlim MT, Mattevi BS, Belmonte-de-Abreu P, Crow TJ (2003): The etiology of schizophrenia and the origin of language: Overview of a theory. Compr Psychiatry 44:7–14.

Bis JC, DeCarli C, Smith AV, van der Lijn F, Crivello F, Fornage M, Debette S, Shulman JM, Schmidt H, Srikanth V, et al. (2012): Common variants at 12q14 and 12q24 are associated with hippocampal volume. Nat Genet 44:545–551.

Boles DB, Barth JM (2011): "Does degree of asymmetry relate to performance?" A critical review. Brain Cogn 76:1–4.

Clark GM, Crow TJ, Barrick TR, Collinson SL, James AC, Roberts N, Mackay CE (2010): Asymmetry loss is local rather than global in adolescent onset schizophrenia. Schizophr Res 120:84–86.

Concha ML, Burdine RD, Russell C, Schier AF, Wilson SW (2000): A nodal signaling pathway regulates the laterality of neuroanatomical asymmetries in the zebrafish forebrain. Neuron 28: 399–409.

Concha ML, Signore IA, Colombo A (2009): Mechanisms of directional asymmetry in the zebrafish epithalamus. Semin Cell Dev Biol 20:498–509.

Crinion J, Turner R, Grogan A, Hanakawa T, Noppeney U, Devlin JT, Aso T, Urayama S, Fukuyama H, Stockton K, et al. (2006): Language control in the bilingual brain. Science 312:1537–1540.

de Guibert Cm, Maumet C, Jannin P, Ferre, Treguier C, Barillot C, Le Rumeur E, Allaire C, Biraben A (2011): Abnormal functional lateralization and activity of language brain areas in typical specific language impairment (developmental dysphasia). Brain 134:3044–3058.

DeLisi LE, Sakuma M, Kushner M, Finer DL, Hoff AL, Crow TJ (1997): Anomalous cerebral asymmetry and language processing in schizophrenia. Schizophr Bull 23:255–271.

Draganski B, Kherif F, Kloppel S, Cook PA, Alexander DC, Parker GJ, Deichmann R, Ashburner J, Frackowiak RS (2008): Evidence for segregated and integrative connectivity patterns in the human Basal Ganglia. J Neurosci 28:7143–7152.

Fischl B, Salat DH, Busa E, Albert M, Dieterich M, Haselgrove C, van der Kouwe A, Killiany R, Kennedy D, Klaveness S, et al.

(2002): Whole brain segmentation: Automated labeling of neuroanatomical structures in the human brain. Neuron 33:341–355.

Franke B, Vasquez AA, Veltman JA, Brunner HG, Rijpkema M, Fernandez G (2010): Genetic variation in CACNA1C, a gene associated with bipolar disorder, influences brainstem rather than gray matter volume in healthy individuals. Biol Psychiatry 68:586–588.

Frasnelli E, Vallortigara G, Rogers LJ (2012): Left-right asymmetries of behaviour and nervous system in invertebrates. Neurosci Biobehav Rev 36:1273–1291.

Friederici AD (2006): What's in control of language? Nat Neurosci 9:991–992.

Gil Robles S, Gatignol P, Capelle L, Mitchell MC, Duffau H (2005): The role of dominant striatum in language: A study using intraoperative electrical stimulations. J Neurol Neurosurg Psychiatry 76:940–946.

Good CD, Johnsrude IS, Ashburner J, Henson RNA, Friston KJ, Frackowiak RSJ (2001): A voxel-based morphometric study of ageing in 465 normal adult human brains. Neuroimage 14:21–36.

Grahn JA, Parkinson JA, Owen AM (2008): The cognitive functions of the caudate nucleus. Prog Neurobiol 86:141–155.

Hayashi Y, Nihonmatsu-Kikuchi N, Hisanaga S-i, Yu X-j, Tatebayashi Y (2012): Neuropathological similarities and differences between schizophrenia and bipolar disorder: A flow cytometric postmortem brain study. PLoS One 7:e33019.

Hegenscheid K, Kuhn JP, Volzke H, Biffar R, Hosten N, Puls R (2009): Whole-body magnetic resonance imaging of healthy volunteers: Pilot study results from the population-based SHIP study. Rofo 181:748–759.

Hou G, Yang X, Yuan TF (2013): Hippocampal asymmetry: Differences in structures and functions. Neurochem Res 38:453–460.

Howie B, Fuchsberger C, Stephens M, Marchini J, Abecasis GR (2012): Fast and accurate genotype imputation in genome-wide association studies through pre-phasing. Nat Genet 44:955–959.

Howie BN, Donnelly P, Marchini J (2009): A flexible and accurate genotype imputation method for the next generation of genome-wide association studies. PLoS Genet 5:19.

Ikram MA, Fornage M, Smith AV, Seshadri S, Schmidt R, Debette S, Vrooman HA, Sigurdsson S, Ropele S, Taal HR, et al. (2012): Common variants at 6q22 and 17q21 are associated with intracranial volume. Nat Genet 44:539–544.

Kawakami R, Shinohara Y, Kato Y, Sugiyama H, Shigemoto R, Ito I (2003): Asymmetrical allocation of NMDA receptor epsilon2 subunits in hippocampal circuitry. Science 300:990–994.

Knecht S, Deppe M, Drager B, Bobe L, Lohmann H, Ringelstein EB, Henningsen H (2000): Language lateralization in healthy right-handers. Brain 123:74–81.

Lee PH, O'Dushlaine C, Thomas B, Purcell SM (2012): INRICH: Interval-based enrichment analysis for genome wide association studies. Bioinformatics 28:1797–1799.

Lehericy S, Ducros M, Van de Moortele PF, Francois C, Thivard L, Poupon C, Swindale N, Ugurbil K, Kim DS: Diffusion tensor fiber tracking shows distinct corticostriatal circuits in humans. Ann Neurol 55:522–529.

Li Y, Willer CJ, Ding J, Scheet P, Abecasis GR (2010): MaCH: Using sequence and genotype data to estimate haplotypes and unobserved genotypes. Genet Epidemiol 34:816–834.

Maltbie E, Bhatt K, Paniagua B, Smith RG, Graves MM, Mosconi MW, Peterson S, White S, Blocher J, El-Sayed M, et al. (2012): Asymmetric bias in user guided segmentations of brain structures. Neuroimage 59:1315–1323.

McGraw KO, Wong SP (1996): Forming inferences about some intraclass correlation coefficients. Psychol Methods 1:30–46.

Medland SE, Duffy DL, Wright MJ, Geffen GM, Hay DA, Levy F, van-Beijsterveldt CEM, Willemsen G, Townsend GC, White V, et al. (2009): Genetic influences on handedness: Data from 25,732 Australian and Dutch twin families. Neuropsychologia 47:330–337.

Morey RA, Petty CM, Xu Y, Hayes JP, Wagner HR, Lewis DV, Labar KS, Styner M, McCarthy G (2009): A comparison of automated segmentation and manual tracing for quantifying hippocampal and amygdala volumes. Neuroimage 45:855–866.

Morey RA, Selgrade ES, Wagner HR, Huettel SA, Wang LH, McCarthy G (2010): Scan-rescan reliability of subcortical brain volumes derived from automated segmentation. Hum Brain Mapp 31:1751–1762.

Nugent AC, Luckenbaugh DA, Wood SE, Bogers W, Zarate CA Jr., Drevets WC (2012): Automated subcortical segmentation using FIRST: Test-retest reliability, interscanner reliability, and comparison to manual segmentation. Hum Brain Mapp 19: 22068.

Ocklenburg S, Gunturkun O (2012): Hemispheric asymmetries: The comparative view. Front Psychol 3:5.

Patenaude B, Smith SM, Kennedy DN, Jenkinson M (2011): A Bayesian model of shape and appearance for subcortical brain segmentation. Neuroimage 56:907–922.

Pearson TA, Manolio TA (2008): How to interpret a genome-wide association study. JAMA 299:1335–1344.

Purcell S, Neale B, Todd-Brown K, Thomas L, Ferreira MA, Bender D, Maller J, Sklar P, de Bakker PI, Daly MJ, et al. (2007): PLINK: A tool set for whole-genome association and population-based linkage analyses. Am J Hum Genet 81:559–575.

Qiu A, Wang L, Younes L, Harms MP, Ratnanather JT, Miller MI, Csernansky JG (2009): Neuroanatomical asymmetry patterns in individuals with schizophrenia and their non-psychotic siblings. Neuroimage 47:1221–1229.

Rabbee N, Speed TP (2006): A genotype calling algorithm for affymetrix SNP arrays. Bioinformatics 22:7–12.

Renteria ME, Stein JL, Johnson K, Medland SE, McMahon KL, De Zubicaray GI, Montgomery GW, Thompson PM, Martin NG, Wright MJ (2011): Genetics of cerebral asymmetry in the caudate nucleus. Poster presentation ASHG 2011, October 2011.

Renteria ME, Wallace A, Strike L, Johnson K, Hibar DP, Stein JL, De Zubicaray G, McMahon KL, Montgomery GW, Thompson PM, et al. (2012): Genetics of left- and right-hemisphere subcortical structures in the human brain. Poster presentation ASHG 2012, November 2012.

Schrimsher GW, Billingsley RL, Jackson EF, Moore BD (2002): Caudate nucleus volume asymmetry predicts attention-deficit hyperactivity disorder (ADHD) symptomatology in children. J Child Neurol 17:877–884.

Shaw P, Lalonde F, Lepage C, Rabin C, Eckstrand K, Sharp W, Greenstein D, Evans A, Giedd JN, Rapoport J (2009): Development of cortical asymmetry in typically developing children and its disruption in attention-deficit/hyperactivity disorder. Arch Gen Psychiatry 66:888–896.

Sherwood CC, Gordon AD, Allen JS, Phillips KA, Erwin JM, Hof PR, Hopkins WD (2011): Aging of the cerebral cortex differs between humans and chimpanzees. Proc Natl Acad Sci USA 108:13029–13034.

Shi F, Liu B, Zhou Y, Yu C, Jiang T (2009): Hippocampal volume and asymmetry in mild cognitive impairment and Alzheimer's

disease: Meta-analyses of MRI studies. Hippocampus 19:1055–1064.

Shrout PE, Fleiss JL (1979): Intraclass correlations: Uses in assessing rater reliability. Psychol Bull 86:420–428.

Sleiman PMA, Satterthwaite T, Ruparel K, Kim C, Chiavacci R, Calkins ME, Gur RC, Gur RE, Hakonarson H (2012): Genome-wide association of structural MRI data in a large, normally developing, pediatric population. Poster presentation ASHG 2012, November 2012.

Stein JL, Medland SE, Vasquez AA, Hibar DP, Senstad RE, Winkler AM, Toro R, Appel K, Bartecek R, Bergmann O, et al. (2012): Identification of common variants associated with human hippocampal and intracranial volumes. Nat Genet 44: 552–561.

The 1000 Genomes Project Consortium (2010): A map of human genome variation from population-scale sequencing. Nature 467:1061–1073.

Toga AW, Thompson PM (2003): Mapping brain asymmetry. Nat Rev Neurosci 4:37–48.

Uhlikova P, Paclt I, Vaneckova M, Morcinek T, Seidel Z, Krasensky J, Danes J (2007): Asymmetry of basal ganglia in children with attention deficit hyperactivity disorder. Neuro Endocrinol Lett 28:604–609.

Visscher PM, Brown MA, McCarthy MI, Yang J (2012): Five years of GWAS discovery. Am J Hum Genet 90:7–24.

Volzke H, Alte D, Schmidt CO, Radke D, Lorbeer R, Friedrich N, Aumann N, Lau K, Piontek M, Born G, et al. (2011): Cohort profile: The study of health in Pomerania. Int J Epidemiol 40: 294–307.

Watkins KE, Paus T, Lerch JP, Zijdenbos A, Collins DL, Neelin P, Taylor J, Worsley KJ, Evans AC (2001): Structural asymmetries in the human brain: A voxel-based statistical analysis of 142 MRI scans. Cerebral Cortex 11:868–877.

Willer CJ, Li Y, Abecasis GR (2010): METAL: Fast and efficient meta-analysis of genomewide association scans. Bioinformatics 26:2190–2191.

Willford J, Day R, Aizenstein H, Day N (2010): Caudate asymmetry: A neurobiological marker of moderate prenatal alcohol exposure in young adults. Neurotoxicol Teratol 32: 589–594.

Wonderlick JS, Ziegler DA, Hosseini-Varnamkhasti P, Locascio JJ, Bakkour A, van der Kouwe A, Triantafyllou C, Corkin S, Dickerson BC (2009): Reliability of MRI-derived cortical and subcortical morphometric measures: Effects of pulse sequence, voxel geometry, and parallel imaging. Neuroimage 44:1324–1333.

Yamashita K, Yoshiura T, Hiwatashi A, Noguchi T, Togao O, Takayama Y, Nagao E, Kamano H, Hatakenaka M, Honda H (2011): Volumetric asymmetry and differential aging effect of the human caudate nucleus in normal individuals: A prospective MR imaging study. J Neuroimaging 21:34–37.

Zatorre RJ, Evans AC, Meyer E, Gjedde A (1992): Lateralization of phonetic and pitch discrimination in speech processing. Science 256:846–849.